Int. J. Heat Mass Transfer. Vol. 29, No. 12, pp. 1943–1951, 1986
Printed in Great Britain

0017-9310/86 \$3.00+0.00
Pergamon Journals Ltd.

Melting of frozen, porous media contained in a horizontal or a vertical, cylindrical capsule

J. A. WEAVER and R. VISKANTA

Heat Transfer Laboratory, School of Mechanical Engineering,
Purdue University, West Lafayette, IN 47907, U.S.A.

(*Received* 23 *May* 1985 *and in final form* 17 *March* 1986)

Abstract—Melting of ice in porous media has been investigated experimentally and analytically for a horizontal and vertical cylindrical capsule. Quantitative results of the temperature distribution and solid–liquid interface motion and shape were obtained for inward melting with different size and types of spherical beads used as the porous media. Predictions from an analysis which considers conduction as the only mode of heat transfer in both the solid and liquid were compared to experimental data to show where natural convection becomes significant. It was found that the melting rate was augmented by natural convection in the liquid. For large differences in the thermal conductivity of the phase-change material and porous medium (e.g. water and aluminum), the effective thermal conductivity of the system was not predicted accurately by the model used, resulting in a further discrepancy between data and predictions. Moreover, the assumption of local temperature equilibrium between the void constituent and the porous medium becomes invalid for a water–aluminum bead system.

INTRODUCTION

In recent years, the heat transfer processes which occur during solid–liquid phase change have received considerable attention due to a wide range of geophysical and engineering applications, and some up-to-date reviews are available [1–4]. Solid–liquid phase change in porous media has been identified as an area of interest for practical applications [5]. However, relatively little attention has been given to the problem because of the inherent complexity encountered when dealing with porous media coupled with phase transformation and motion of the interface.

Goldstein and Reid [6] have investigated melting (or freezing) in water-saturated, porous media in the presence of a seepage flow. Using techniques of complex variable theory, the energy equation in the unfrozen region was solved for without knowing the shape of the frozen region. The nonlinear interfacial energy balance was transformed into a nonlinear integro-differential equation which was then linearized by solving it over short time increments until the frozen region either vanishes or reaches its equilibrium shape. Okada and Fukumoto [7] have studied melting of frozen, porous media around a horizontal tube and accounted for natural convection in the melt. Momentum equations, which were based on Darcy's law for fluid flow in porous media, together with an energy equation, were solved numerically using an implicit finite-difference scheme; the results were compared to experimental data and fair agreement was reported.

Due to the limited amount of analytical and experimental work on phase-change heat transfer in liquid-saturated, porous media reported to date, the various effects are not fully understood and a number of critical issues remain unresolved. These effects of natural convection in the liquid, porosity of the medium, differences in the thermophysical properties of the porous medium and phase-change material (PCM), subcooling of the solid PCM and superheating of the liquid PCM have not been systematically studied.

The purpose of this paper is to report experimental data and to examine if natural convection during melting of frozen porous media is an important mode of heat transfer. To this end, melting experiments have been performed in both a vertical and a horizontal cylindrical capsule filled with different size glass and aluminum beads and with ice (water) as the PCM. Comparison of experimental data with predictions based on a one-dimensional model in which heat is transferred only by conduction is used to show when natural convection becomes significant.

EXPERIMENTS

Experimental apparatus

Melting experiments with frozen porous media were performed in the cylindrical capsule shown in Fig. 1. The capsule consists of a brass cylinder (73.0 mm ID, 1.07 mm wall thickness and 158.8 mm long) with a bottom and top cap made of acrylic plastic. The capsule could be operated with the axis both in vertical and horizontal orientations. The thermal conductivity of acrylic is less than the thermal conductivity of the PCM and porous medium which helps to reduce end effects. The heat source/sink consisted of two copper tubes (6.35 mm OD, 4.76 mm ID) wrapped and soldered around the outside of the brass cylinder with the

NOMENCLATURE

c	specific heat
d	bead diameter [mm]
Fo	Fourier number, $\alpha_{sm}t/R^2$
H	axial length of the test section
Δh_f	latent heat-of-fusion
k	thermal conductivity
L	liquid thickness
r	radius
r_l	radial interface position
R	outside radius of test section
Ste	Stefan number for melting, $c_l(T_f - T_w)/\Delta h_f$
t	time
T	temperature
z	axial direction.

Greek symbols

α	thermal diffusivity, $k/\rho c$
γ	dimensionless axial distance, z/H
δ	dimensionless interface position, r_l/R
η	dimensionless liquid thickness, L/R
θ	dimensionless temperature, $(T - T_w)/(T_f - T_w)$
ξ	dimensionless radius, r/R
ρ	density
τ	dimensionless time, $FoSte$
ϕ	porosity.

Subscripts

f	fusion state
i	initial state
l	liquid-phase properties
lm	effective liquid properties
m	porous medium properties
s	solid-phase properties
sm	effective solid properties
w	wall.

two tube inlets each at opposite ends of the cylinder. In this manner, the double-wrapped tubing acts like a counter-flow heat exchanger to give a uniform wall temperature. The test cell was insulated using Styrofoam fitted around the heat exchanger and caps. A detailed description of the apparatus is given elsewhere [8].

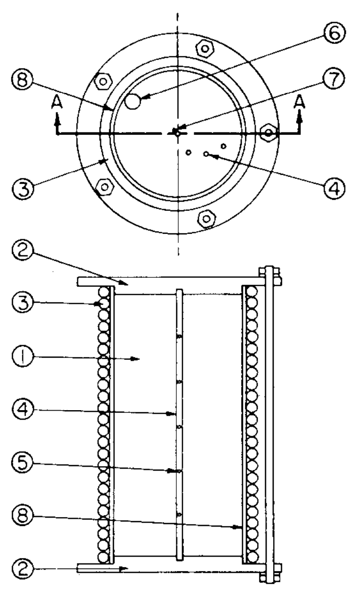

FIG. 1. Schematic of test cell; 1—test section; 2—acrylic end caps; 3—copper heat exchanger; 4—thermocouple rake; 5—thermocouple position on rakes; 6—fill tube; 7—overflow tube; 8—brass cylinder.

Measurement of the temperature distribution and wall temperature was made respectively by four thermocouple rakes and five thermocouples placed on the outside of the brass cylinder using thermal epoxy. Radial and azimuthal position of the rakes are shown in Fig. 1. This rake arrangement allows temperature measurements to be affected little by a rake at a larger radius. The copper–constantan thermocouples had a wire diameter of 0.13 mm, and the bead was placed approximately 0.5 mm away from the rake and directed radially outward.

Test materials

Two different types of spherical beads were used as the porous media. The soda-lime glass beads had diameters of 1.59, 2.89 and 6.0 mm. The properties used were for a soda-lime glass with a chemical composition as close as could be obtained to the chemical composition of the glass beads used in this study. The aluminum was commercially pure (Type 1100) with a bead diameter of 3.18 mm. Again, the properties were for an aluminum of chemical composition as close as possible to the aluminum bead used in this study [8]. The PCM was once-distilled, degasified water.

The porosity (volume of voids over the total volume) was determined in two ways using a separate cylindrical container. The porosity of the aluminum bead was 0.39 and for the largest glass bead size was 0.38 (0.36 for the smaller sizes). The porosity for all sizes of spherical beads should be equal, assuming the same packing arrangement. The discrepancy is due to the roundness of the beads and increase in porosity near the wall of the container which is more significant for the larger bead size [9].

Test procedure and data reduction

In preparing for an experiment, the test cell was first filled with the porous media. The balls were settled to obtain approximately the same conditions for each test. After degasification, the water was carefully siphoned into the test cell to ensure that no air is trapped in the matrix and to prevent air from mixing with the water. A mixture of alcohol and water was circulated through the heat exchanger from two constant-temperature baths to solidify the liquid. After complete solidification and after uniform initial conditions were established, melting of the ice was initiated.

The thermocouple output was read at a given interval of time using a data logger. From these temperatures, the temperature distributions and solid–liquid interface position as a function of time were determined. The time at which the interface reaches an arbitrary thermocouple, i.e. radial position, is determined as the time when the thermocouple temperature is markedly different between two consecutive temperature readings. Since the temperature readings are taken at finite intervals, this introduces some error in the experimental determination of the solid–liquid interface motion and position. The interface position could not be photographed and the flow structure in the melt could not be visualized due to the scattering of light by the porous medium.

ANALYSIS

Assumptions and model equations

The physical system modeled for melting consists of a cylinder, closed at the ends, filled uniformly with spheres (porous media) and solid PCM. Initially, the system is at a uniform temperature less than or equal to the fusion temperature $T_i \leqslant T_f$. At time $t \geqslant 0$, a uniform temperature is imposed on the inside of the cylinder wall which is greater than the fusion temperature, $T_w > T_f$. This initiates the melting process with the fusion front moving radially inward.

The following assumptions are made in the analysis:

(1) The porous media is isotropic and homogeneous.
(2) Physical properties are independent of temperature.
(3) Overall volume change due to phase change is negligible.
(4) Heat conduction is the only mode of heat transfer in both the solid and the liquid (i.e. natural convection is absent).
(5) The solid–liquid interface is clearly defined, i.e. the PCM has a well-defined fusion temperature.
(6) The local temperatures of the phase in the voids and porous medium are the same.
(7) Porosity is constant.

With the preceding assumptions, the resulting dimensionless energy equations for the solid and liquid are, respectively

$$Ste\frac{\partial \theta_{sm}}{\partial \tau} = \frac{1}{\xi}\frac{\partial}{\partial \xi}\left(\xi\frac{\partial \theta_{sm}}{\partial \xi}\right) \tag{1}$$

$$Ste\left(\frac{\alpha_{sm}}{\alpha_{lm}}\right)\frac{\partial \theta_{lm}}{\partial \tau} = \frac{1}{\xi}\frac{\partial}{\partial \xi}\left(\xi\frac{\partial \theta_{lm}}{\partial \xi}\right). \tag{2}$$

The initial, boundary and interface conditions for melting are:

$$\theta_{sm} = \theta_i \quad \text{for } \tau \leqslant 0 \tag{3a}$$

$$\theta_{lm} = \theta_w = 0 \quad \text{at } \xi = 1 \tag{3b}$$

$$\theta_{sm} = \theta_{lm} = 1 \quad \text{at } \xi = \delta \tag{3c}$$

$$\phi\frac{\rho_s c_l}{(\rho c)_{sm}}\frac{\partial \delta}{\partial \tau} = \left(\frac{k_{lm}}{k_{sm}}\right)\frac{\partial \theta_{lm}}{\partial \xi} - \frac{\partial \theta_{sm}}{\partial \xi} \quad \text{at } \xi = \delta \tag{3d}$$

$$\frac{\partial \theta_{sm}}{\partial \xi} = 0 \quad \text{at } \xi = 0. \tag{3e}$$

Before the model equations can be solved, a viable means of determining the thermophysical properties of the porous media is needed. Generally, there can be any combination of solids and fluids when dealing with porous media. As such, an effective or average set of properties is used which are based on the void fraction (porosity) of each constituent. Specifically, the effective thermal capacitance (density times specific heat) is needed, which results in the following equation for the solid [10]:

$$(\rho c)_{sm} = (\rho c)_m(1-\phi)+(\rho c)_s\phi \tag{4}$$

where sm, m and s refer respectively to the solid influenced by the porous media, the porous medium and the solid phase. The equation for the liquid is determined by simply replacing sm and s by lm and l, respectively.

The thermal conductivity is more complex because it depends on the geometry, heat flow direction and volume of each constituent. Various effective thermal conductivity models based on geometrical considerations or empirical results have been proposed [10]. Also, Veinberg [11] derived an equation which he claimed to be universally applicable for randomly distributed spherical inclusions in a medium. The thermal conductivity equation for the Veinberg model is

$$k_{sm}+\phi\left(\frac{k_m-k_s}{k_s^{1/3}}\right)k_{sm}^{1/3}-k_m = 0. \tag{5}$$

A sensitivity study was performed [8] using five different thermal conductivity models to determine which best represents the system. From the temperature distribution and solid–liquid interface position data, it was found that the Veinberg model gave the best agreement for both a water–aluminum and water–glass bead system.

Method of solution

When solving a moving-boundary heat transfer problem numerically, complications arise due to the motion of the solid–liquid interface with time. As such, the position of the interface is not known *a priori* and the domain over which the energy equations are solved varies. Furthermore, there exists a discontinuity in the temperature gradient at the fusion front.

Briefly, the method of solution uses a fixed grid system coupled with an implicit time scheme. Murray and Landis [12] first proposed a fixed grid method of solution. Similarly, a node is specified at the interface and the interface position must be determined as it progresses through the nodal system. To eliminate the inaccuracy introduced by the interpolation or extrapolation [12], unequal spacing in the computational grid on both sides of the interface (which changes with time) is used. To handle this unequal spacing, the energy equation for the solid and liquid phases are finite-differenced by first multiplying by the radius ξ and then integrating over a unit control volume in space [13].

Finite-differencing of the interfacial energy balance requires an accurate approximation for the first derivative of temperature using the unequal spacing at the interface. By twice differentiating a second-order polynomial and solving for the first derivative (e.g. solid side of the interface), a suitable formula was derived which uses the interface node and two adjacent nodes on the solid side of the interface.

Initially ($t < 0$), there is no solid phase present. Assuming that the fusion front velocity is proportional to the amount of energy removed at the cylinder wall, a dimensionless energy balance at the wall derived similar to the preceding interfacial energy balance yields

$$\phi \frac{\rho_s c_l}{(\rho c)_{sm}} \frac{\partial \xi}{\partial \tau} = \frac{\partial \theta_{sm}}{\partial \xi}. \tag{6}$$

This energy balance was used in the numerical solution to determine an initial fusion front velocity (i.e. solid thickness). After the solid phase is established, the interfacial energy balance must be used. The purpose of the wall energy balance is to initiate the numerical solution.

The independence of the solution on the grid was established by performing calculations for different grids. The results reported in the paper were obtained with a grid of 25 nodal points. The model equations were also solved for the limiting case of a homogeneous medium (no porous media, $\phi = 1.0$). The numerical results obtained for the interface position were found to be in excellent agreement with numerical predictions reported in the literature for melting [14] assuming that heat transfer in the solid and liquid is only by conduction. This established confidence in the numerical algorithm employed.

RESULTS AND DISCUSSION

Temperature distributions

Figures 2 and 3 show the variation of temperature with time at different radial and axial locations for a glass bead diameter of 6.0 and 1.59 mm, respectively. Bead size makes a significant difference in the temperature distributions. The effects of natural convection become more important as the bead diameter increases due to the increasing permeability of the porous system (for approximately the same porosity). An empirical correlation for the permeability of packed beds of the same diameter spheres is given by Bear [15]. Based on the expression for uniform size spherical beads, the permeabilities for 1.59, 2.89 and 6.0 mm diameter glass beads are found to be 1.60×10^{-9} m^2, 5.28×10^{-9} m^2 and 2.85×10^{-8} m^2, respectively. Since there appears to be no unique characteristic length for a porous medium in which the phase-change boundary is moving, the Rayleigh number is not given. However, the imposed test cell wall temperature is contained in the Stefan number (*Ste*) specified in the figure captions, and therefore the Rayleigh number can be calculated for the system.

Figure 2 shows that natural convection is very important for a bead diameter of 6.0 mm as evidenced by the high liquid temperatures at $\gamma = 0.84$ (upper portion of the vertical test cell orientation) which approach the wall temperature ($\theta = 0$). The temperatures increase from the bottom to the top of the capsule, and this difference is greater as the melt thickness increases (radius decreases). This clearly indicates that the fluid motion due to natural convection is up along the wall and down along the solid–liquid interface. Poor agreement between data and the pre-

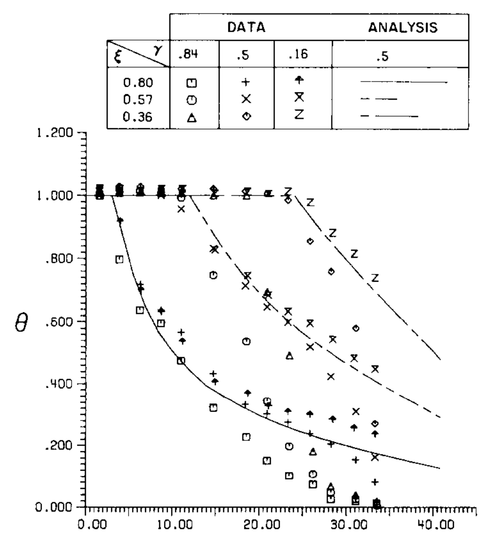

FIG. 2. Comparison of predicted and measured temperatures for melting of ice: glass beads 6.0 mm in diameter, $\theta_i = 1.0$, $Ste = 0.186$.

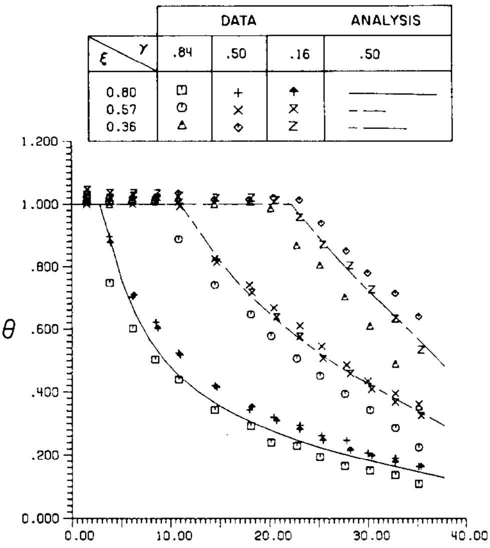

FIG. 3. Comparison of predicted and measured temperatures for melting of ice: glass beads 1.59 mm in diameter, $\theta_i = 1.0$, $Ste = 0.185$.

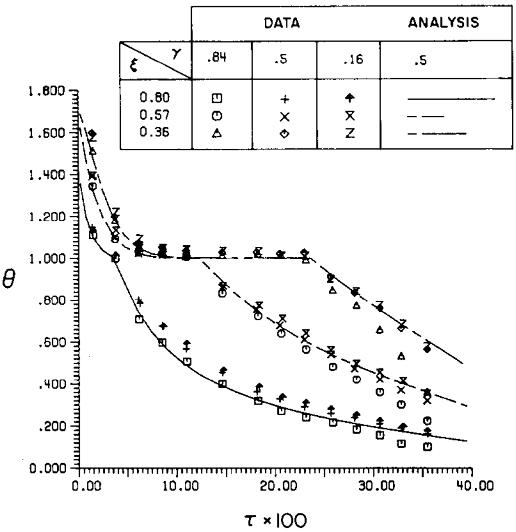

FIG. 4. Comparison of predicted and measured temperatures for melting of ice for some subcooling of the solid PCM: glass beads 2.89 mm in diameter, $\theta_i = 2.145$, $Ste = 0.185$.

dictions based on the pure conduction heat transfer model provide further evidence of the natural convection effects. Note that natural convection is absent initially and the melting is conduction dominated. The fluid circulation due to natural convection is considerably less intense for a bead diameter of 1.59 mm (Fig. 3). The temperature difference between the top and bottom of the vertical capsule is considerably smaller, and agreement between data and predictions is better.

The temperature variation with time for an initially subcooled system is shown in Fig. 4. There is good agreement for the solid temperatures, and the liquid temperatures reveal natural convection effects in the melt. Again, natural convection does not appear until later times and becomes more dominant as the melt thickness increases.

The effects of natural convection are markedly different when the cylinder axis is oriented horizontally (Fig. 5). There is little variation in the temperature distributions for the various axial locations, with the exception that the water added to the system from the reservoir increased the temperature at $\gamma = 0.84$, because the water temperature was warmer than that of the wall due to insufficient cooling. This results in the difference between the temperatures at $\gamma = 0.84$, 0.5 and 0.16 being smaller (approximately equal within the measurement accuracy of the thermocouples used) than the typical temperature differences for a vertically oriented cylinder. The symbol T (or top) refers to the thermocouple rakes being positioned above the axis of the capsule with the rake closest to the wall rotated 15° from the vertical. The symbol B (or bottom) means the thermocouple rakes have been rotated 180° from the vertical such that they are below the axis of the test cell. As would be expected, the liquid temperatures in the upper half of the test section are higher than those in the bottom half due to the upward motion of the fluid caused by the natural convection.

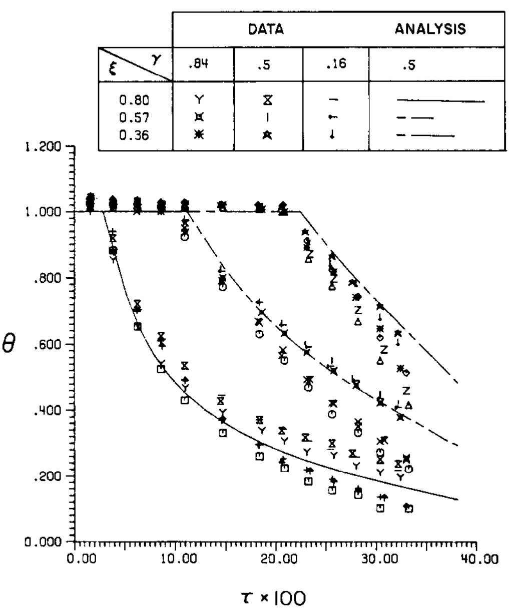

FIG. 5. Comparison of predicted and measured temperatures for melting with the test cell oriented horizontally: glass beads 2.89 mm in diameter, $\theta_i = 1.0$, $Ste = 0.186$ with rakes at top and $Ste = 0.185$ with rakes at bottom. (Note: The data points indicated on the figure are for thermocouple rakes located on the bottom of the test cell. The symbols for the data points when the thermocouple rakes are located at the top of the test cell are identical to those given in Fig. 4.)

The temperature distribution for melting in an ice–aluminum bead system is shown in Fig. 6. The analysis overpredicts the temperature because the Veinberg [11] model overestimates the effective thermal conductivity. Since there is a large difference in the properties of the PCM and porous media, the temperature variation is markedly different from that of an ice–glass bead system. The temperature does not vary as smoothly as that for an ice–glass bead system, and the difference between the axial temperatures becomes smaller as the liquid thickness increases.

Solid–liquid interface position

Good agreement between predictions and data for the temperature distribution will result in good agreement for the solid–liquid interface position, since they are intimately related. Figure 7 illustrates the variation of the melt layer thickness with time for glass beads (2.89 mm in diameter) and aluminum beads (3.17 mm in diameter). The agreement is much better for the ice–glass bead system, because the thermal conductivity of the porous media and PCM are similar, but the model underpredicts the melting rate. The melting rate of the ice–glass bead system is influenced more by natural convection than the ice–aluminum bead system. For melting, addition of the PCM to the test section has no effect if the water is at the same temperature as the wall (i.e. it just fills the void formed by the melting of ice). As expected from the temperature distributions, the local melting rate is slowest at the bottom of the vertical capsule and progressively increases upward (the top melts the quickest). Due to the high thermal conductivity of the aluminum bead, conduction is more significant during melting. Note that the top and

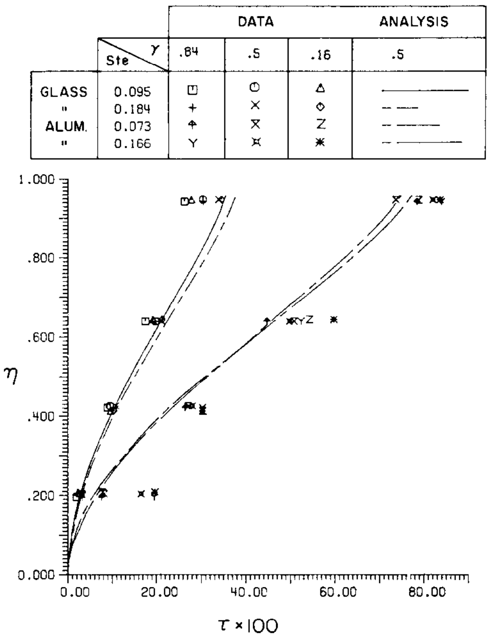

FIG. 7. Effect of Stefan number on the liquid layer thickness for melting of ice in vertically oriented capsule: glass beads 2.89 mm in diameter, aluminum beads 3.18 mm in diameter, $\theta_i = 1.0$.

bottom portions melt at the same rate, and the spread in the data is approximately the same (at three of the four locations). The model overpredicts the melting rate because of the effective thermal conductivity model used.

In both systems, complete melting is quicker for the larger Stefan number. Natural convection effects are significant for both Stefan numbers for an ice–glass bead system. The agreement is better for the smaller Stefan number with aluminum beads as the porous media (data trend is similar to the shape of the predicted curve). The slower melting rate allows the system to approach local temperature equilibrium between the PCM and the porous media. Conduction-controlled melting appears to be dominant for the smaller Stefan number, but not to the same extent as that for the larger Stefan number.

The bead size makes a significant difference in the melting rate for an ice–glass bead system (Fig. 8). Melting is quickest for the larger bead size and slowest for the small diameter bead due to the different permeabilities of the porous media as discussed earlier. For the larger permeability, the fluid motion is more intense because the resistance to flow is smaller. Note, the spread in the data is greatest for the large bead diameter, which indicates that natural convection effects are more important. The beads greatly suppress natural convection. Comparison of the model predictions with data for melting without porous media can be found elsewhere [8].

Effects of an initial subcooling of the solid on the

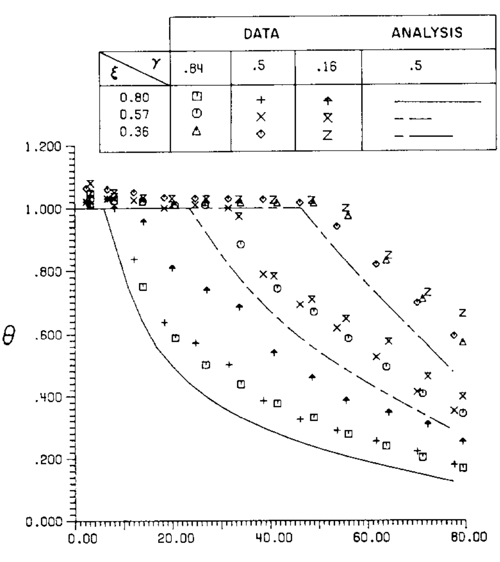

FIG. 6. Comparison of predicted and measured temperatures for melting of ice in a vertically oriented capsule: aluminum beads 3.18 mm in diameter, $\theta_i = 1.0$, $Ste = 0.166$.

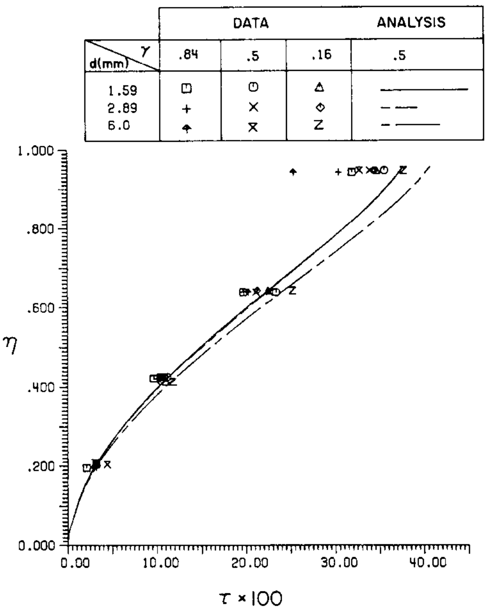

FIG. 8. Effect of glass bead diameter on the liquid layer thickness for melting of ice in a vertically oriented capsule, $\theta_i = 1.0$, $Ste = 0.185$ for $d = 1.59$ mm, $Ste = 0.184$ for $d = 2.89$ mm and $Ste = 0.186$ for $d = 6.0$ mm.

interface position are shown in Fig. 9. As predicted, the initial subcooling slows down the melting rate. Due to slightly better agreement between predictions and data for an initially subcooled ice, it appears that the natural convection effects are not as important due to heat addition to the solid required to raise its temperature to the fusion temperature.

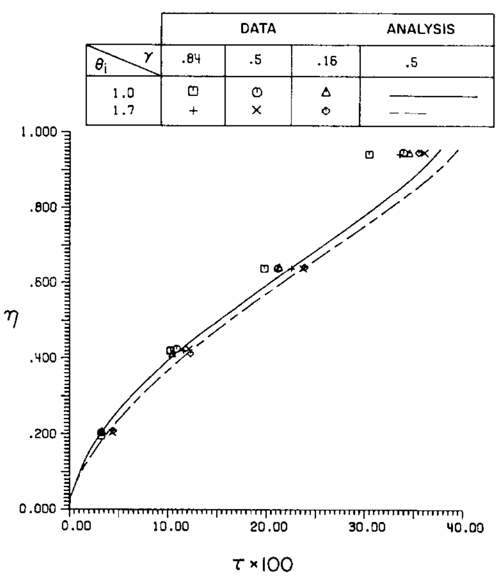

FIG. 9. Effect of the initial temperature on the liquid layer thickness for melting of ice in a vertically oriented capsule: glass beads 2.89 mm in diameter, $Ste = 0.184$ for $\theta_i = 1.0$ and $Ste = 0.185$ for $\theta_i = 1.7$.

The test cell orientation has a marked effect on the melting rate as shown in Fig. 10. Note that the melting rate at $\gamma = 0.84$ for the horizontal orientations was slightly greater than it should be due to the added water not being sufficiently cooled to the wall temperature. For the vertically oriented test cell, the fluid temperature increases as the liquid moves up along the hot wall and decreases as the liquid flows down along the solid–liquid interface due to the natural convection circulation. The melting rate is greatest at the top of the solid–liquid interface and steadily decreases downward. The temperature distribution for the horizontally oriented test cell (Fig. 5) shows that the melt temperature is larger above the solid, which suggests that the fluid motion is from the bottom to the top of the solid. Due to the different and changing length of the solid–liquid interface for each orientation that the fluid is exposed to (which corresponds to the amount the fluid is cooled and the melting rate), the melting rates for the two orientations are different along the axis of the test cell. For the vertical orientation, the fluid motion is along the axis of the capsule. Therefore, the length of the interface that the fluid is in contact with is approximately constant (neglecting the slight curvature due to more melting at the top). In contrast for the horizontal orientation, the fluid motion is around the circumference of the solid which continuously decreases until the solid is completely melted. Therefore, melting is faster at $\gamma = 0.84$ for the vertically positioned capsule (compared to the horizontal orientation), and

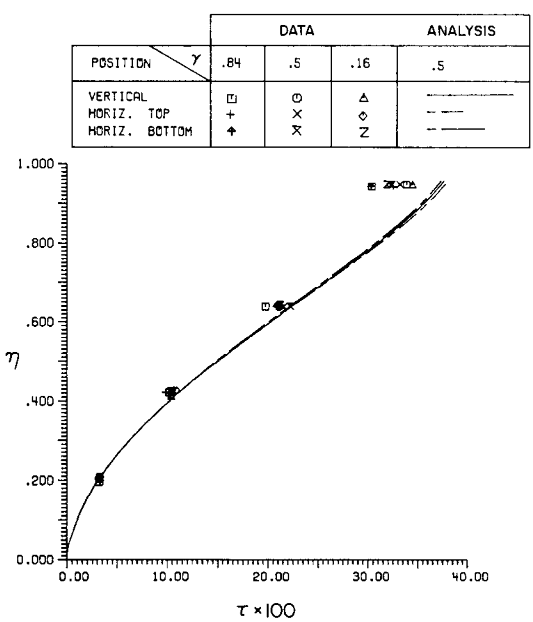

FIG. 10. Effect of test cell orientation on the liquid layer thickness for melting of ice, glass beads 2.89 mm in diameter, $\theta_i = 1.0$; $Ste = 0.184$ for vertical orientation, $Ste = 0.186$ for horizontal orientation with rakes on top and $Ste = 0.185$ for horizontal orientation with rakes on bottom.

melting in the horizontally oriented capsule is faster at $\gamma = 0.5$ and 0.16 (compared to the vertical orientation). The measured melting rate is greater at later times than that predicted based on conduction-controlled heat transfer for both orientations (natural convection becomes more intense). Likewise, the difference in the melting rates between the two orientations becomes greater at later times.

CONCLUSIONS

Natural convection plays an important role during melting of an ice–porous-media system. Melting occurs faster at the top of a vertically oriented cylindrical capsule due to the fluid circulation, with natural convection effects becoming more important as the melt thickness increases. The analysis underpredicts the melting rate for a water-glass-bead system because natural convection was ignored. For a water–aluminum-bead system, the analysis overpredicts the melting rate, because the effective thermal conductivity of the system was overpredicted, and conduction predominates over natural convection.

The results show that the effective thermal conductivity model is adequate only for a system in which the porous medium and PCM have similar values. If the porous medium has a very large thermal conductivity compared to the PCM, the Veinberg model for the effective conductivity is clearly inadequate. Furthermore, the assumption that the PCM and porous medium are in local temperature equilibrium becomes invalid.

The experimental data show that natural convection in the liquid affects the temperature distribution and the interface shape as well as its motion during melting of ice–porous-media systems. Natural convection in the liquid needs to be modeled for a realistic prediction of temperature distribution and melt front motion. Theoretical work is currently under way and will be reported in the near future.

Acknowledgements—This research was supported, in part, by the National Science Foundation Heat Transfer Program under Grant MEA-8313573. The authors are indebted to Professor W. Leidenfrost for many helpful discussions.

REFERENCES

1. R. Viskanta, Natural convection in melting and solidification. In *Natural Convection: Fundamentals and Applications* (Edited by S. Kakac, W. Aung and R. Viskanta), pp. 845–877. Hemisphere, Washington, DC (1985).
2. R. Viskanta, Phase change heat transfer. In *Solar Heat Storage: Latent Heat Materials* (Edited by G. A. Lane), Vol. 1, pp. 153–221. Uniscience Edn, CRC Press, Boca Raton, FL (1983).
3. V. J. Lunardini, *Heat Transfer in Cold Climates*. Van Nostrand Reinhold, New York (1981).
4. M. N. Özişik, *Heat Conduction*. John Wiley, New York (1980).
5. K. E. Torrance, R. J. Schoenhals, C. L. Tien and R. Viskanta, Natural convection in porous media, *Proc. Workshop on Natural Convection*, University of Notre Dame, Notre Dame, IN, pp. 36–45 (1982).
6. M. E. Goldstein and R. L. Reid, Effect of fluid on freezing and thawing of saturated porous media, *Proc. R. Soc.* **364A**, 45–73 (1978).
7. M. Okada and T. Fukumoto, Melting around a horizontal pipe embedded in a frozen porous medium, *Trans. Japan Soc. mech. Engrs* **48B**, 2041–2049 (1982) (in Japanese).
8. J. A. Weaver, Solid–liquid phase change heat transfer in porous media. MSME thesis, Purdue University (1985).
9. B. C. Chandrasekhara and D. Vortmeyer, Flow model for velocity distribution in fixed porous beds under isothermal conditions, *Warme- u. Stoffubertr.* **12,** 105–111 (1979).
10. M. A. Combarnous and S. A. Bories, Hydrothermal convection in saturated porous media. In *Advances in Hydroscience*, Vol. 10, pp. 231–307. Academic Press, New York (1975).
11. A. K. Veinberg, Permeability, electrical conductivity, dielectric constant and thermal conductivity of a medium with spherical and ellipsoidal inclusions, *Sov. Phys. Dokl.* **11,** 593–595 (1967).
12. W. D. Murray and F. Landis, Numerical and machine solutions of transient heat conduction problems involving melting or freezing, *J. Heat Transfer* **81,** 106–112 (1959).
13. S. V. Patankar, *Numerical Heat Transfer and Fluid Flow*. McGraw-Hill, New York (1980).
14. E. M. Sparrow and J. A. Broadbent, Freezing in a vertical tube, *J. Heat Transfer* **105,** 217–225 (1983).
15. J. Bear, *Dynamics of Fluids in Porous Media*. American Elsevier, New York (1972).

FUSION D'UN MILIEU POREUX GELE CONTENU DANS UNE CAPSULE CYLINDRIQUE HORIZONTALE OU VERTICALE

Résumé—La fusion de la glace dans un milieu poreux est étudiée expéritalement et analytiquement pour une capsule cylindrique horizontale ou verticale. Des résultats quantitatifs de la distribution de température et du mouvement et de la déformation de l'interface sont obtenus pour la fusion interne avec différentes dimensions et formes de lits de sphères utilisés comme milieux poreux. Des prévisions d'une analyse qui considère la conduction comme le seul mode de transfert thermique sont comparées aux données expérimentales pour montrer que la convection naturelle est sensible. On trouve que la vitesse de fusion est augmentée par la convection naturelle dans le liquide. Pour de grandes différences dans la conductivité thermique du matériau qui change d'état et du milieu poreux (ici eau et aluminium), la conductivité thermique effective du système n'est pas prévue correctement par le modèle utilisé, ce qui conduit à un écart entre les données expérimentales et les prévisions. L'hypothèse d'un équilibre local de température entre le fluide intersticiel et le milieu poreux devient incorrecte pour le système eau–aluminium.

SCHMELZEN VON GEFRORENEN, PORÖSEN STOFFEN

Zusammenfassung—Der Schmelzvorgang von Eis in einem porösen Stoff wurde experimentell und analytisch in einer horizontalen und vertikalen zylindrischen Kapsel untersucht. Die Temperaturverteilung, die Wanderungsgeschwindigkeit sowie die Gestalt der Schmelzfront wurden für den Fall des Abschmelzens im Inneren quantitativ ermittelt, wobei unterschiedliche kugelförmige Perlen als poröses Material verwendet wurden. Analytische Befunde, wonach Wärmeleitung den einzigen Transportmechanismus sowohl in der Flüssigkeit, als auch im Feststoff darstellt, wurden mit den experimentellen Ergebnissen verglichen um zu erkennen, inwiefern natürliche Konvektion für den Vorgang bedeutsam ist. Es konnte gezeigt werden, daß die Schmelzrate durch auftretende natürliche Konvektion zunimmt. Bei großen Unterschieden der Wärmeleitfähigkeiten von Phasenwechselmaterial und porösem Material (zum Beispiel Wasser und Aluminium), konnte die effektive Wärmeleitfähigkeit des Systems nicht mehr hinreichend genau durch das verwendete Modell beschrieben werden, wodurch sich weitere Abweichungen zwischen Berechnung und Versuch ergaben. Desweiteren ist die Annahme eines örtlichen Temperaturgleichgewichts zwischen Hohlraumkomponente und porösem Medium für das System Wasser–Aluminiumperlen nicht mehr gerechtfertigt.

ПЛАВЛЕНИЕ ЗАМОРОЖЕННЫХ ПОРИСТЫХ СРЕД, СОДЕРЖАЩИХСЯ В ГОРИЗОНТАЛЬНЫХ И ВЕРТИКАЛЬНЫХ ЦИЛИНДРИЧЕСКИХ КАПСУЛАХ

Аннотация—Экспериментально и аналитически исследуется плавление льда в пористой среде в горизонтальных и вертикальных цилиндрических капсулах. Количественные результаты по распределению температуры, движению и форме границ раздела твердое тело-жидкость получены для случая внутреннего плавления при различных размерах и типах сферических шариков, используемых в качестве пористой среды. Расчеты, проведенные при условии, что происходит только индуктивный перенос тепла в твердом теле и жидкости, сравнивались с данными эксперимента для выделения случаев, когда существенной становится естественная конвекция. Найдено, что интенсивность плавления увеличивается при естественной конвекции в жидкости. Если теплопроводности среды, в которой осуществляются фазовые превращения, и пористого скелета существенно различаются (например, вода и алюминий) значение эффективной теплопроводности системы рассчитывалось по модели с некоторым загрублением, что приводит к дальнейшему расхождению между экспериментальными данными и расчетами. Более того, предположение о локальном равновесии температур между пустотами и пористым скелетом для системы вода-алюминиевые шарики утрачивает справедливость.